

## Electronic Supplementary Information

### **Harnessing hydrogen evolution reaction (HER) through electrical mobility of embossed Ag(I)-molecular cage and Cu(II)-coordination polymer**

*Ananya Debnath,<sup>a</sup> Sangharaj Diyali,<sup>a</sup> Mainak Das,<sup>b</sup> Subhrajyoti Panda,<sup>c</sup> Debasish Mondal,<sup>d</sup> Debasis Dhak,<sup>d</sup> Chandra Shekhar Purohit,<sup>c</sup> Partha Pratim Roy,<sup>b</sup> and Bhaskar Biswas<sup>\*a</sup>*

---

<sup>a</sup>*Department of Chemistry, University of North Bengal, Darjeeling-734013, India.*

<sup>b</sup>*Department of Chemistry, Jadavpur University, Kolkata-700032, India.*

<sup>c</sup>*Department of Chemical Sciences, National Institute of Science Education and Research, Bhubaneswar 752050, India.*

<sup>d</sup>*Department of Chemistry, Sidho-Kanho-Birsha University, Purulia-723104, India*

\*Corresponding author. E-mail: [bhaskarbiswas@nbu.ac.in](mailto:bhaskarbiswas@nbu.ac.in)

## Contents

A. <b>Experimental</b> .....	S4-S8
i. Synthetic Procedure.....	S4-S5
ii. Physical measurements.....	S5-S6
iii. X-ray crystallography.....	S6
iv. Device fabrication.....	S6-S7
v. Electrode preparation .....	S7
iv. Electrochemical measurements.....	S7
v. Calculation of active sites and turnover frequency (TOF).....	S8
B. <b>Characterization</b> .....	S7-S11
i. FT-IR, NMR,UV-vis Spectroscopic characterization .....	S8-S9
ii. Electrical characterization.....	S9-S11
C. <b>Figures</b> .....	S12-S21
i. IR spectra.....	S12
ii. UV-Vis spectra.....	S12
iii. <sup>1</sup> H NMR.....	S13
iv. <sup>13</sup> C NMR.....	S13
v. <sup>1</sup> H NMR of <b>Ag<sub>MOC</sub></b> .....	S14
vi. <sup>1</sup> H NMR of <b>Cu<sub>CP</sub></b> .....	S14
vii. The ESI-MS measurement of <b>HL</b> in presence of <b>Cu<sup>2+</sup></b> ion.....	S15
viii. Packing diagram and long-range supramolecular framework .....	S15
ix. Tauc's Plot.....	S16
x. dV/d(lnI) vs. I and H(I) vs. I curve.....	S16
xi. Capacitance versus frequency plot for <b>Ag<sub>MOC</sub></b> (red) and <b>Cu<sub>CP</sub></b> .....	S17
xii. CV of bare GC electrode, <b>Ag<sub>MOC</sub></b> and <b>Cu<sub>CP</sub></b> .....	S17
xiii. Tafel plot of the <b>Ag<sub>MOC</sub></b> and <b>Cu<sub>CP</sub></b> .....	S18
xiv. CPE measurement of <b>Ag<sub>MOC</sub></b> and <b>Cu<sub>CP</sub></b> in 1M KOH media.....	S19
xv. Multiple CVs cycle of <b>Ag<sub>MOC</sub></b> and <b>Cu<sub>CP</sub></b> in 1M KOH media.....	S19
xvi. DLS plot of <b>Ag<sub>MOC</sub></b> and <b>Cu<sub>CP</sub></b> before and after HER study.....	S19
xvii. PXRD diagram of <b>Ag<sub>MOC</sub></b> and <b>Cu<sub>CP</sub></b> before and after HER study.....	S20

xviii. FESEM images of <b>Ag<sub>MOC</sub></b> and <b>Cu<sub>CP</sub></b> after HER study.....	S20
xix. UV-Vis spectra of the recovered <b>Ag<sub>MOC</sub></b> and <b>Cu<sub>CP</sub></b> after HER study in DMSO...S21	S21
xx. LSV of parent metal salts, AgNO <sub>3</sub> and Cu(OAc) <sub>2</sub> at 5 mV/s in 1M KOH.....	S21
<b>C. Tables.....</b>	<b>S22-S24</b>
i. Crystallographic structural parameters of <b>Ag<sub>MOC</sub></b> and <b>Cu<sub>CP</sub></b> .....	S22
ii. Selected bond angles and distances for <b>Ag<sub>MOC</sub></b> .....	S23
iii. Selected bond angles and distances for <b>Cu<sub>CP</sub></b> .....	S23
iv. Schottky Diode Parameters.....	S24
v. SCLC/Charge Transport Parameters.....	S24
vi. HER performance parameter.....	S24
<b>References.....</b>	<b>S25</b>

## A. Experimental

### i. Synthetic Procedure

#### Chemicals

All chemicals and solvent used in the synthesis were the analytical reagent grade (AR), and of the highest purity available. >98.0% pure o-anisaldehyde (TCI, Japan), >97.0% pure 1,3-diaminopropan-2-ol (TCI, Japan), copper acetate monohydrate (SDFCL, India), AgNO<sub>3</sub> (Merck, India) were purchased from monetary outlets. All the solvent were used as received without further purification.

#### Synthesis of the Schiff base ligand (HL)

Under the ambient condition, o-anisaldehyde (0.816 g, 6 mmol) was heated under reflux with 1,3-diaminopropan-2-ol (0.222 g, 3 mmol) in 40 ml ethanolic solution. After 10 h, the pale yellow reaction solution was evaporated under reduced pressure to yield a gummy mass. Further, the product was purified through column chromatography using a hexane-ethyl acetate eluant mixture and dried under vacuum and stored over CaCl<sub>2</sub> for subsequent use. Yield, 0.910 g (87.7%). Anal. Calc. for C<sub>19</sub>H<sub>21</sub>N<sub>2</sub>O<sub>3</sub> (HL): C, 69.92; H, 6.79; N, 8.58. Found: C, 69.92; H, 6.92; N, 8.58%. <sup>1</sup>H NMR δ (ppm): 3.87 (s, 3H), 3.94(s, 1H), 6.91-7.99(Ar-H, 4H), 8.80(s,1H). <sup>13</sup>C NMR δ (ppm): 55.5, 65.2, 71.2, 111.0, 120.7, 124.5, 127.3, 132.0, 158.8, 159.0. IR (KBr, cm<sup>-1</sup>): 1090 (s), 1249 (s), 1639 (s) UV-Vis (λ max, nm): 260(0.94), 306(0.60)

#### Synthesis of Cu<sub>CP</sub> and Ag<sub>MOC</sub>

In two different reaction sets, the aq. methanolic solution of Cu(OAc)<sub>2</sub> (0.40 g, 2 mmol) and AgNO<sub>3</sub>(0.35 g, 2 mmol) were added dropwise under magnetic stirring in a respective methanolic

solution of **HL** (0.32 g, 1 mmol) for 30 min. The bright blue color was observed for former reaction solution and the latter remained nearly colorless. Further, ammonium thiocyanate (0.15 g, 2 mmol) was added slowly to the blue reaction mixture of  $\text{Cu}(\text{OAc})_2$  and **HL**. Finally, both the reactions were filtered and supernatant liquids for the respective reaction mixtures were kept in ambient condition for slow evaporation. After few days, blue crystals of **Cu<sub>CP</sub>** and nearly colourless **Ag<sub>MOC</sub>** crystals were separated out. The crystals were washed with hexane and isolated.

Yield for **Cu<sub>CP</sub>**: 0.37 g (69% for 1 based on metal salt). Anal. Calc. for  $\text{C}_{3.5}\text{H}_{5.5}\text{CuN}_2\text{O}_{1.5}\text{S}$  (1): C, 21.25; H, 2.58; N, 16.52. Found: C, 21.25; H, 2.58; N, 16.52. IR (KBr,  $\text{cm}^{-1}$ ): 2085 (S-C  $\equiv$  N), 1638(COO, asymmetric stretching) 1427 (COO, symmetric stretching); UV-Vis ( $\lambda$ , nm,  $10^{-5}$  M, DMSO): 233 (0.83), 277 (1.10), 363 (0.132).

Yield for **Ag<sub>MOC</sub>**: 0.37 g (69% for 1 based on metal salt). Anal. Calc. for  $\text{C}_{19}\text{H}_{22}\text{AgN}_4\text{O}_3,(\text{NO}_3)$  (1): C, 52.55; H, 5.11; N, 4.82. Found: C, 45.51; H,5.11; N,6.45%. IR (KBr,  $\text{cm}^{-1}$ ): 1638(C=N), 1034, 1249 (C-O); UV-Vis ( $\lambda$ ,nm, $10^{-5}$ M, DMSO): 233 (0.77), 309 (0.47).

### Physical measurements

FT-IR spectra of **HL** and the synthetic compounds were recorded using an FTIR-8400S SHIMADZU spectrometer in the range of 400-3600  $\text{cm}^{-1}$ .  $^1\text{H}$  and  $^{13}\text{C}$  NMR spectra of the synthetic compounds were obtained on a Bruker Advance 400 MHz spectrometer in  $\text{CDCl}_3$  at 298 K. Steady-state absorption spectral data were measured with a HITACHI U-2910 spectrophotometer. A Perkin Elmer 2400 CHN microanalyser was employed to carry out the elemental analyses of the compounds. The morphology and structural characteristics of the synthetic compounds were determined by powder X-ray diffractometer (Rigaku SmartLab) using  $\text{Cu-K}_\alpha$  radiation ranging from  $10^\circ$ - $80^\circ$ . The size and shape of the nano-materials were assessed through scanning electron

microscopy (JSM IT500HR, Japan) images. Electron dispersive X-ray (EDX) spectral analysis was also carried out to reveal the %elemental contribution as well as the purity of the materials. An RVL PG-Lyte-1.0 potentiostat consisting of a glassy-carbon working electrode, Pt counter electrode, and Ag/AgCl reference was employed to study the electrochemical analysis of the compounds. N<sub>2</sub> adsorption analyses have been performed at 77 K using a liquid nitrogen bath (77 K) on a Quantachrome Quadrasorb automatic volumetric instrument. The Ag<sub>MOC</sub> and Cu<sub>CP</sub> samples were outgassed for 10 h at 110 °C under a vacuum before the gas adsorption studies. The surface areas are evaluated using the Brunauer-Emmett-Teller (BET) model applied between P/P<sub>0</sub> values of 0.05 and 0.3 for the compounds. Dynamic Light Scattering (DLS) experiments have been performed using Litesizer™ 500 equipped with a 658 nm, 40 mW laser at 25°C with a 10 mm pathlength quartz cuvette.

### **X-ray structural studies and refinement**

Suitable single-crystals of Ag<sub>MOC</sub> and Cu<sub>CP</sub> were selected for single-crystal X-ray diffraction studies. The structural diffraction data were collected on a Bruker-Kappa APEX II CCD diffractometer equipped with a 1 K charge-coupled device (CCD) area detector employing a graphite monochromated Mo-K $\alpha$  radiation ( $k \frac{1}{4} 0.71073 \text{ \AA}$ )<sup>o</sup> at 100.0(2) K. The cell parameters and the reduction and correction of the collected data were determined by SMART SAINTPlus software, respectively<sup>1</sup> followed by SADABS absorption corrections.<sup>2</sup> Finally, the structure was solved by direct method with SHELXL-97 program package.<sup>3</sup> The refinement by full-matrix least-squares method was executed on all F<sup>2</sup> data with SHELXL-97. For all non-hydrogen atoms, anisotropic refinement was performed. Subsequently the additional hydrogen atoms were positioned by riding model.

**Fabrication of Schottky Device.** To fabricate the Schottky device, at first, Indium Tin Oxide (ITO) coated glass substrate was cleaned by acetone, distilled water and isopropanol repeatedly

and sequentially in an ultrasonication bath for 20 min. At the same time, a well-dispersed solution of the  $\text{Cu}_{\text{CP}}$  and  $\text{Ag}_{\text{MOC}}$  in N N-dimethyl formamide (DMF) medium was prepared and spin-coated onto the pre-cleaned ITO-coated glass at 600 rpm for 1 min with the help of SCU 2700 spin coating unit. This spin-coating step was repeated 4 times. After drying in a vacuum, the film thickness was measured as 1  $\mu\text{m}$  by a surface profiler. Aluminum (Al) electrodes were deposited onto the film by a Vacuum Coating Unit 12A4D of HINDHIVAC under a pressure of  $10^{-6}$  Torr. The area of the Al electrodes was maintained as  $7.065 \times 10^{-6}$   $\text{m}^2$  by the shadow mask. The current-voltage measurements of the fabricated device with  $\text{Cu}_{\text{CP}}$  and  $\text{Ag}_{\text{MOC}}$  were carried out by a Keithley 2635B source meter interfaced with PC by a two-probe technique between the voltage range -3V to +3V at room temperature.

**Electrode preparation.** In 2ml vial, 5mg catalyst were weighed and 770  $\mu\text{l}$   $\text{H}_2\text{O}$ , 30  $\mu\text{l}$  Nafion (5 wt%, Sigma Aldrich) and 200  $\mu\text{l}$  EtOH were added using micropipette and left for sonication for 40 min to form a homogenous ink. The electrochemical glassware was oven-dried overnight and cooled prior to operate in the experiment. GCE, as working electrode were polished with Alumina powder (0.05 Microns) of size and interspersed by washings with distilled  $\text{H}_2\text{O}$ . 10  $\mu\text{l}$  ink was drop casted into the as cleaned GCE and dried at 40° C. The mass loading was received as 0.71 mg  $\text{cm}^{-2}$ .

**Electrochemical Measurements.** Hydrogen evolution activity were performed using K-Lyte electrochemical workstation. Cyclic voltammetry (CV), Linear sweep voltammetry (LSV) and chronoamperometry were demonstrated using 1M KOH aqueous solution as supporting electrolyte. In a three-electrode setup, a glassy carbon electrode (GCE, 3 mm diameter) was used as a working electrode, Platinum wire as a counter electrode and Ag/Ag<sup>+</sup> as a reference electrode (saturated with AgCl). The potential region was swept from -0.6V to -1.8V (vs Ag/AgCl) at the

scan rate of 5 mVs<sup>-1</sup>. All the potentials in this study were given with respect to a reversible hydrogen electrode (RHE) by using the Nernst equation  $E(\text{RHE}) = E^0(\text{Ag}/\text{AgCl}) + E(\text{Ag}/\text{AgCl}) + 0.059 \cdot \text{pH}$ . All the data were corrected for  $iR$  loss. All the electrochemical experiment was monitored in ambient condition.

**Calculation of active sites and turnover frequency (TOF).** The active sites and turnover frequency (TOF) were calculated for complex salts **1** and **2** following the equations. Considering one electron reduction process, from the CV the absolute components of voltammetric charges (cathodic and anodic) were examined by analyzing the area of curve of complex salt **1** and **2**. Further the active sites (**n**) of the heterogeneous catalyst were calculated in mol<sup>-1</sup>.

$$\text{Charge ( } Q \text{)} = \frac{\text{Area of the curve}}{2 \times \text{Scan rate}}$$

$$n = \frac{Q}{2 \times F}$$

The turnover frequency (in s<sup>-1</sup>) per-sites were calculated using the equation given below:

$$\text{TOF} = \frac{I}{F n} \frac{1}{2}$$

Where, *I* is current (in A) during the LSV, *F* is Faraday constant (in C mol<sup>-1</sup>), *n* is the number of active sites (in mol) and the factor ½ represents two electron process in hydrogen production.

## **B. Characterization**

### **FT-IR, NMR and UV-Vis spectroscopic characterization**

The molecular composition of the ligand was examined by FT-IR, UV-Vis and NMR analysis. The structural characterization and morphological view of the synthetic **Ag<sub>MOC</sub>** and **Cu<sub>CP</sub>** compounds have been assessed with FT-IR, PXRD and FE-SEM analysis. FT-IR spectroscopy spectral analysis of the **Ag<sub>MOC</sub>** and **HL** exhibited characteristic peaks at 1638 and 1639 cm<sup>-1</sup> respectively attributed to the azomethine stretching frequencies. The presence of peaks at 1034, 1090 and 1249 cm<sup>-1</sup> for the compounds suggests C-O stretching vibrations for **Ag<sub>MOC</sub>** and **HL**. The characteristic peak at 2085 cm<sup>-1</sup> appeared for the presence of S-C≡N stretching frequency, and peaks at 1427 and 1638 cm<sup>-1</sup> represent -COO symmetric and asymmetric stretching frequency respectively for **Cu<sub>CP</sub>**. The compounds were soluble in DMSO, DMF and common polar solvents. The structural compositions of **HL** were examined with various spectral analyses like <sup>1</sup>H and <sup>13</sup>C NMR, FT-IR, UV-Vis. The <sup>1</sup>H NMR of the ligand was recorded in CDCl<sub>3</sub>. The aromatic-proton signals appeared in the range δ6.91 to 7.99 ppm, the chemical shift value at δ8.8 ppm representing the imine protons and the peak at δ 3.82-3.87 representing the methoxy protons for the ligand. The <sup>13</sup>C NMR spectra of **HL** showed the signals at δ159 ppm attributing the presence of the C-atom of the imine while the characteristic signals at δ55.5 ppm correspond to the methoxy C-atom. The chemical shift values of the aromatic-C in **HL** appeared in the range δ 111.0-132.0 ppm. The FT-IR spectral analysis of the exhibited characteristic peaks at 1638 and 1639 cm<sup>-1</sup> for **Ag<sub>MOC</sub>** and **HL** respectively attributed to the azomethine stretching frequencies. The presence of peaks at 1034, 1090 and 1249 cm<sup>-1</sup> for the compounds, respectively suggests C-O stretching vibrations for **Ag<sub>MOC</sub>** and **HL**. The absorption spectra of **HL**, **Ag<sub>MOC</sub>** and **Cu<sub>CP</sub>** were obtained in DMSO medium. **HL**, **Ag<sub>MOC</sub>** displayed high energetic electronic bands in 260 nm and 305-310 nm where as **Cu<sub>CP</sub>** presents a lower intensity and sharp maximum at 260 nm at room temperature. The appearance of these higher energetic electronic bands corresponds to the π→π\*

or  $n \rightarrow \pi^*$  electronic transitions. The notable electronic bands of HL, Ag<sub>MOC</sub>, and Cu<sub>CP</sub> agree well with the literature values.<sup>4,5</sup>

**Electrical Characterization:** The Thermionic Emission (TE) theory is endorsed to take cognizance of the charge transport mechanism in the devices.<sup>6</sup> The current of a diode can be expressed as the following equations according to TE theory.<sup>7</sup>

$$I = I_0 \exp\left(\frac{qV}{\eta kT}\right) \left[ 1 - \exp\left(-\frac{qV}{\eta kT}\right) \right] \quad \dots\dots(S1)$$

Where,

$$I_0 = AA^* T^2 \exp\left(-\frac{q\phi_B}{kT}\right) \quad \dots\dots(S2)$$

$$\phi_B = \frac{kT}{q} \ln\left(\frac{AA^* T^2}{I_0}\right) \quad \dots\dots(S3)$$

Where,  $I_0$  indicates the saturation current,  $q$  represents the electronic charge,  $k$  is the Boltzmann constant,  $T$  is the temperature in Kelvin,  $V$  is the forward bias voltage,  $\eta$  is the ideality factor,  $\phi_B$  is the effective barrier height at zero bias,  $A$  is the diode area ( $7.065 \times 10^{-6} \text{ m}^2$ ),  $A^*$  is the effective Richardson constant ( $1.20 \times 10^6 \text{ Am}^{-2}\text{K}^{-2}$ ). From Cheung, the forward bias I-V characteristics in term of series resistance can be expressed as.<sup>8</sup>

$$I = I_0 \exp\left[\frac{q(V - IR_s)}{\eta kT}\right] \quad \dots\dots(S4)$$

Where, the  $IR_S$  term represents the voltage drop across the series resistance of device. Under this condition, the values of the series resistance can be determined from the following functions using equations (S5 & S6).<sup>9</sup>

According to Cheung's model:

$$\frac{dV}{d\ln(I)} = \left(\frac{\eta kT}{q}\right) + R_S I \quad \dots\dots\dots(S5)$$

$$H(I) = R_S I + \eta \phi_B \quad \dots\dots\dots(S6)$$

and  $H(J)$  can be expressed as:

$$H(I) = V - \left(\frac{\eta kT}{q}\right) \ln\left(\frac{I}{AA^*T^2}\right) \quad \dots\dots\dots(S7)$$

The dielectric constant of two materials is measured from the capacitance vs. frequency plot (C-f) (**Fig. S9**) by the equation<sup>10</sup>:

$$\epsilon_r = \frac{Cd}{\epsilon_0 A} \quad \dots\dots\dots (S8)$$

Transit time ( $\tau$ ) is the time at which time a carrier travels from anode to cathode. It is the sum of the average time spent by an electron as a free carrier plus the total time spent in the tarp. The transit time ( $\tau$ ) of the charge carrier is given by the equation<sup>11</sup>:

$$\tau = \frac{9\epsilon_0\epsilon_r A}{8d} \left(\frac{V}{I}\right) \quad \dots\dots\dots (S9)$$

The longer transit time indicates a higher trapping probability.<sup>12</sup>

### C. Figures

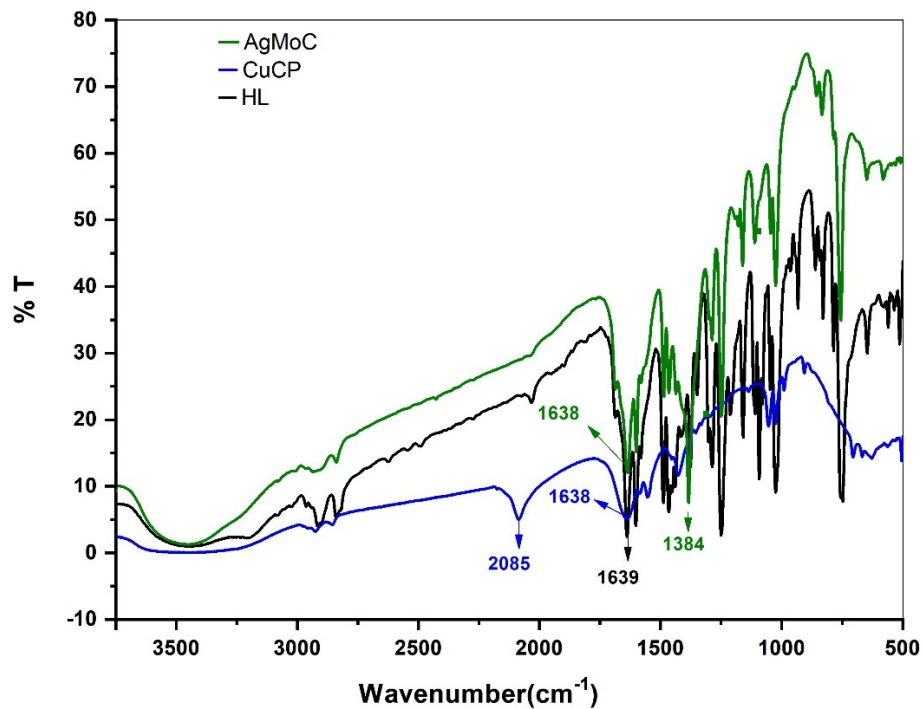
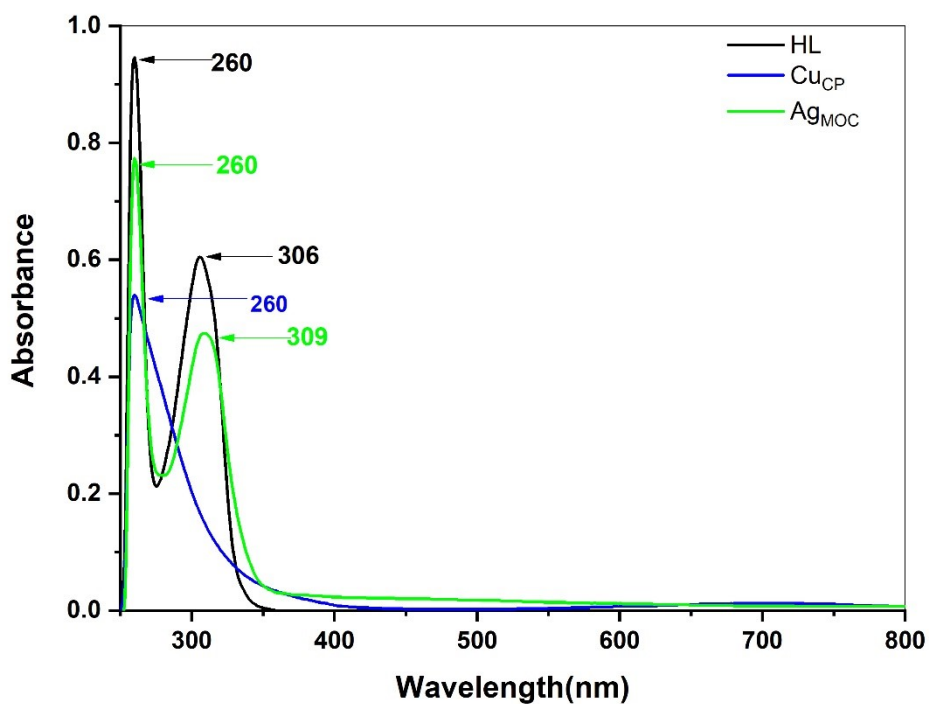
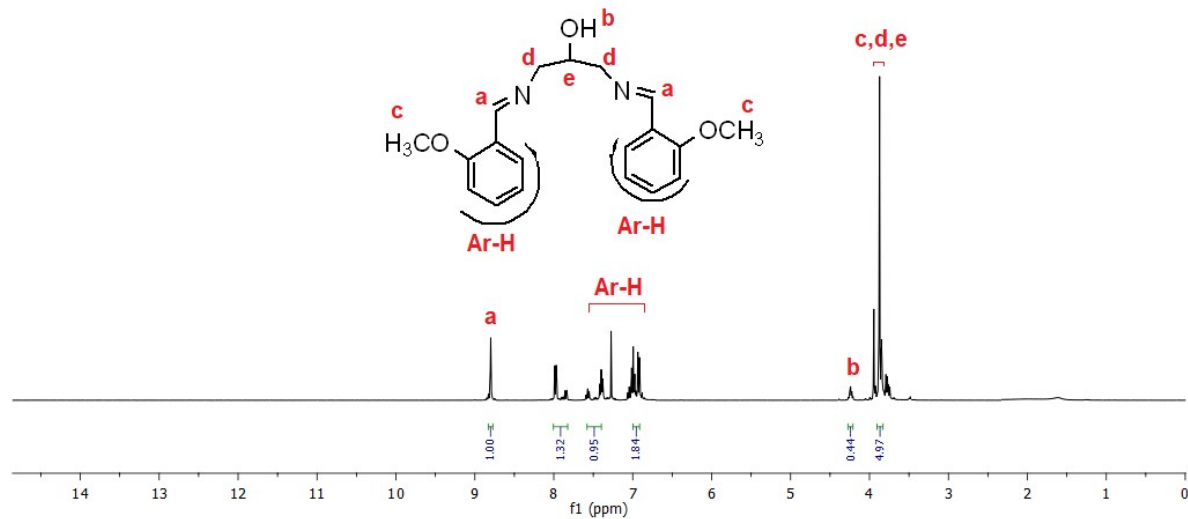


Fig. S1. FT-IR spectra of HL, Cu<sub>CP</sub> and Ag<sub>MOF</sub>



**Fig.S2.** UV-Vis spectra of  $\text{Ag}_{\text{MOC}}$ ,  $\text{Cu}_{\text{CP}}$  and  $\text{HL}$  having  $10^{-5}\text{M}$  concentration in DMSO at RT



**Fig. S3**  $^1\text{H}$  NMR of HL

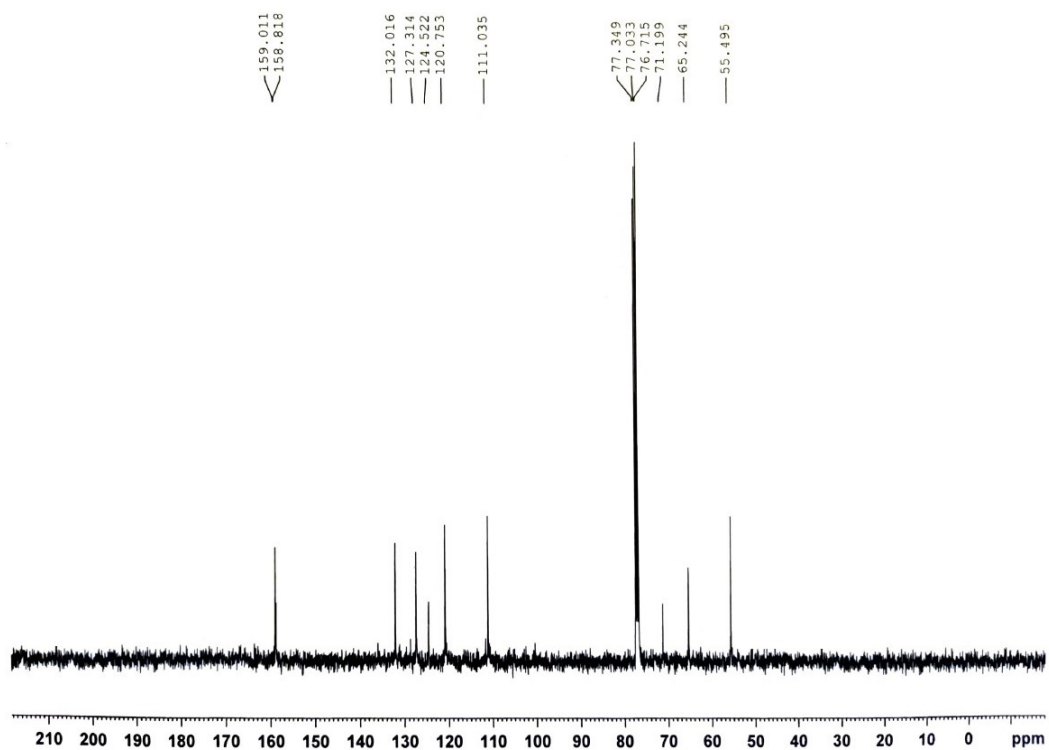


**Fig. S4**  $^{13}\text{C}$  NMR of HL

NBU\_BBiswas2  
Ag-MOC-1H

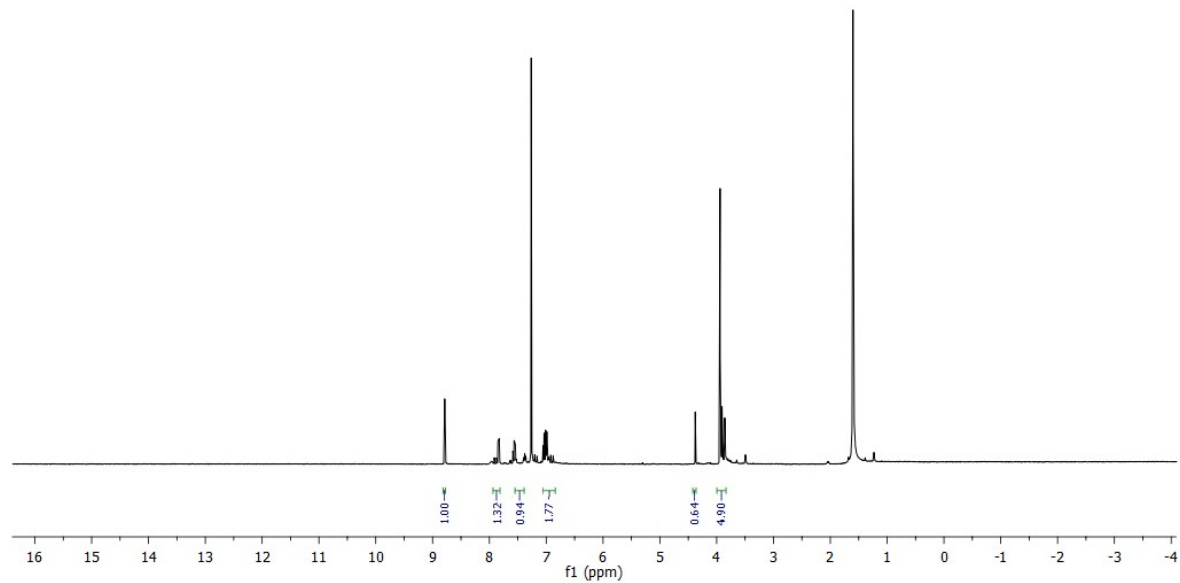


**Fig. S5**  $^1\text{H}$  NMR of Ag<sub>MOC</sub> in DMSO- $d_6$

Cu-CP-1H

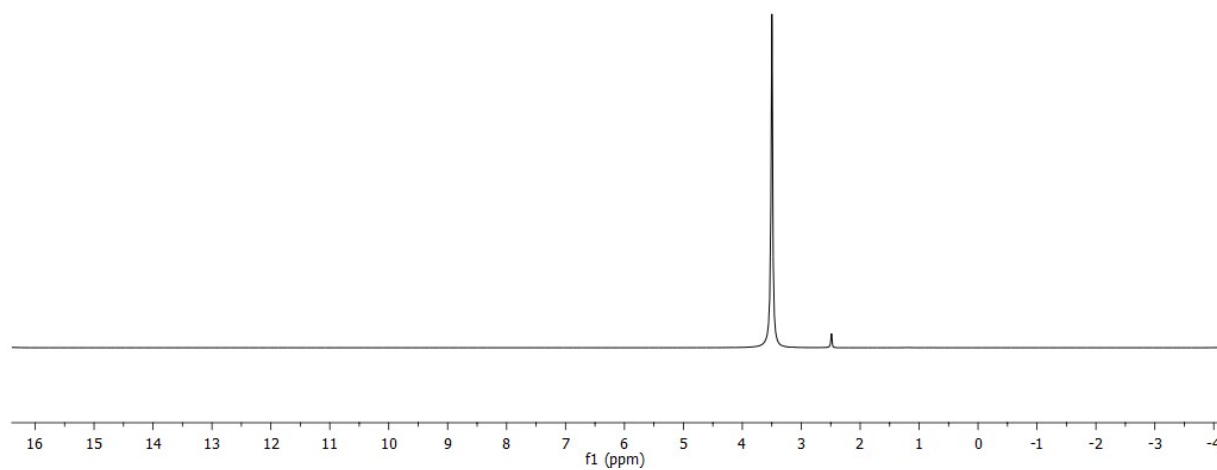


**Fig. S6**  $^1\text{H}$  NMR of Cu<sub>CP</sub> in  $\text{CDCl}_3$

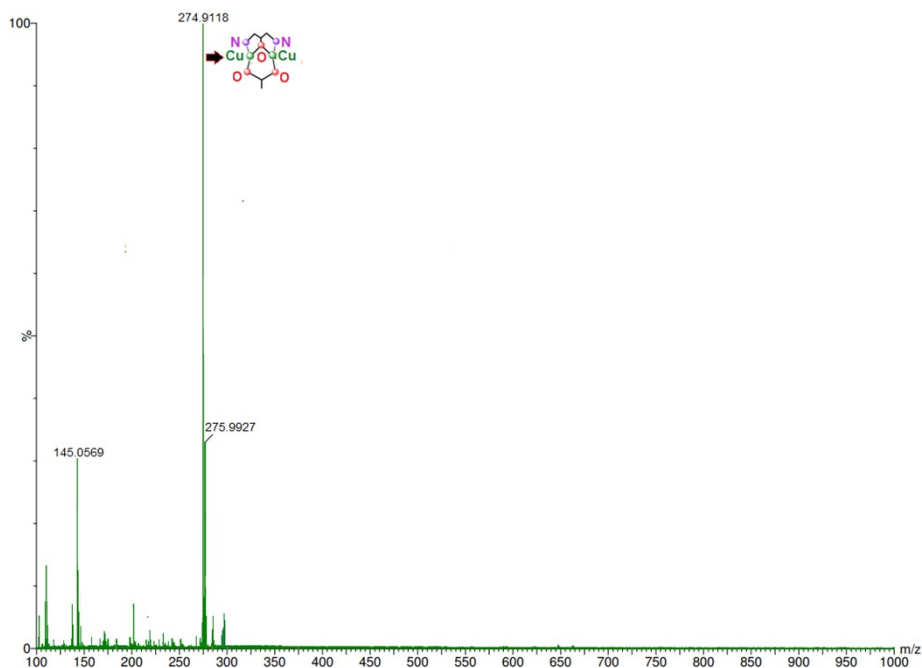


**Fig. S7** ESI-MS of HL upon addition of  $\text{Cu}^{2+}$  salt in aq. methanol (v/v, 2/8)

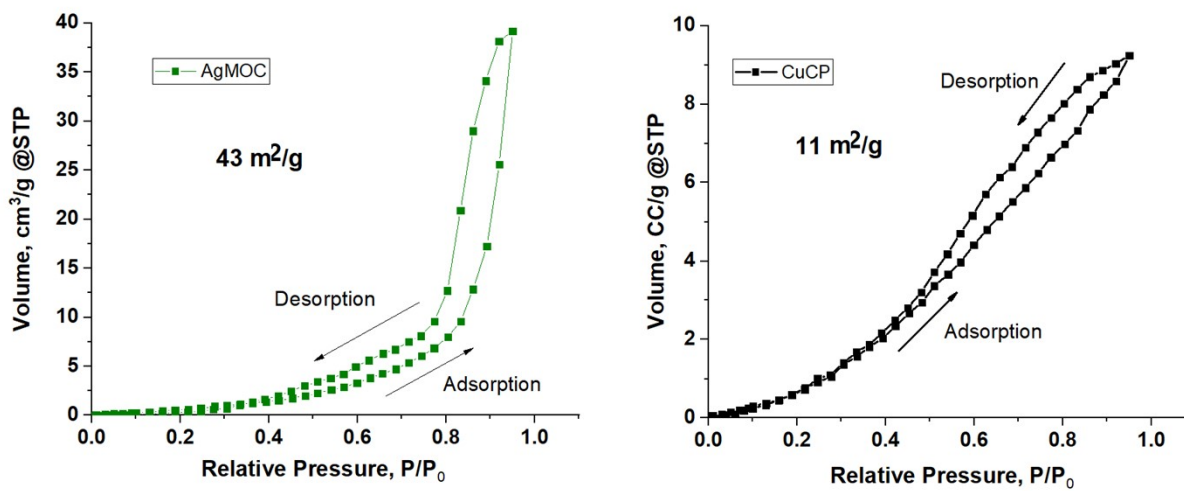


**Fig. S8.** BET isotherm analysis: (left)  $\text{AgMOC}$ , (right)  $\text{CuCP}$

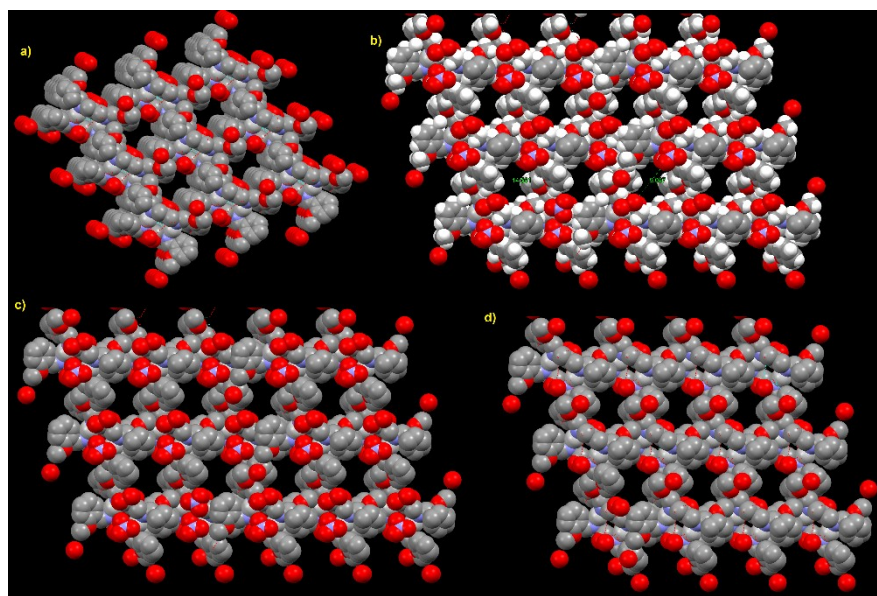


**Fig. S9** (a) Packing diagram; (b) long-range framework including all atoms; (c) supramolecular frameworks without H; (d) supramolecular frameworks without C and nitrate ions

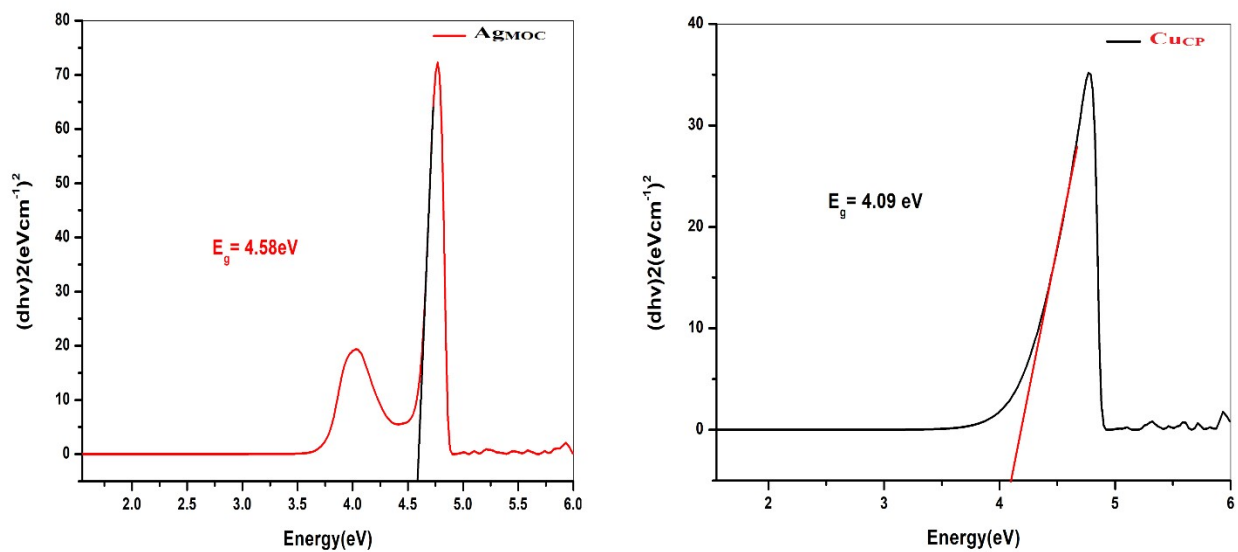


**Fig. S10.** Tauc's Plot for direct band gap energies of (a)AgMOC (b) CuCP

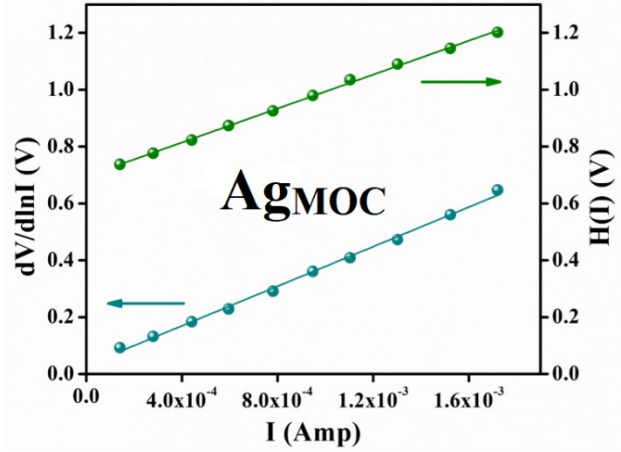
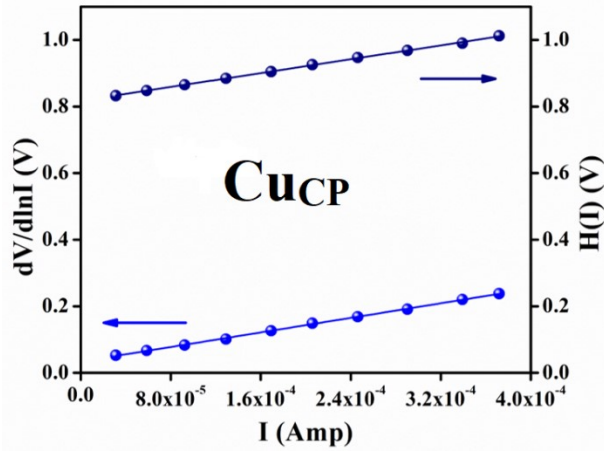


**Fig. S11.**  $dV/d(\ln I)$  vs.  $I$  and  $H(I)$  vs.  $I$  curve for (a)  $\text{Cu}_{\text{CP}}$  and (b)  $\text{Ag}_{\text{MOC}}$  based Schottky barrier diode.

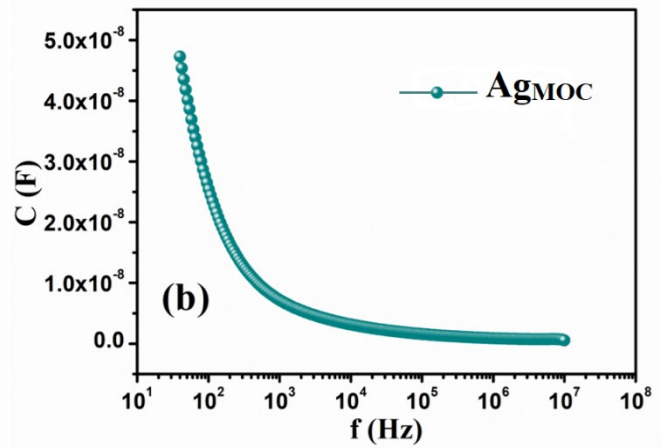
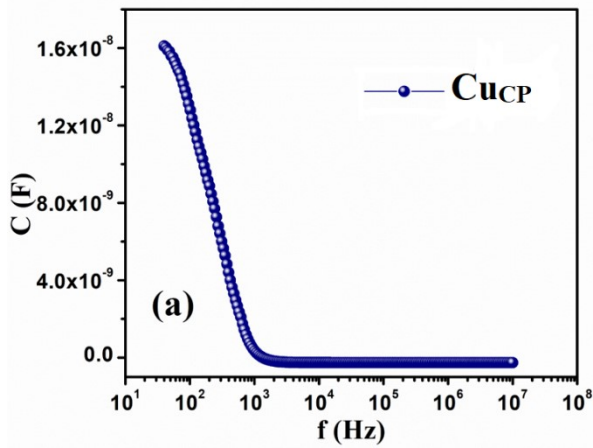


**Fig. S12.** Capacitance versus frequency plot for  $\text{Cu}_{\text{CP}}$  and  $\text{Ag}_{\text{MOC}}$ .

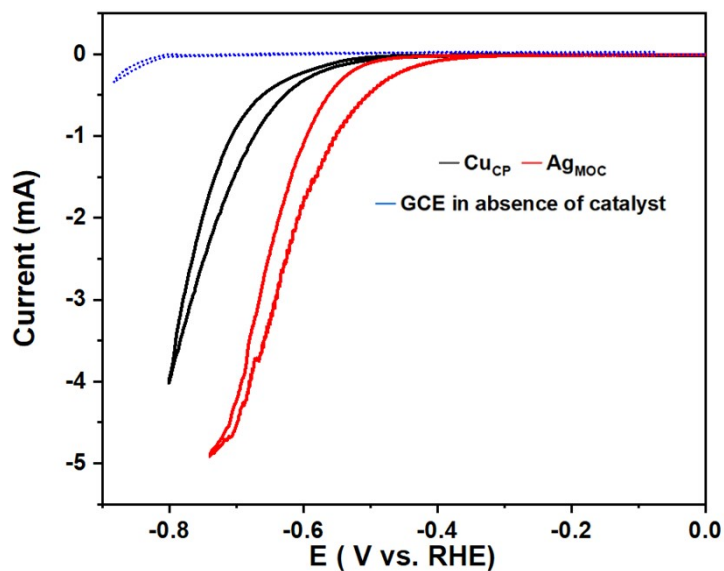


**Fig. S13.** CVs of Complex  $\text{Ag}_{\text{MOC}}$  (red),  $\text{Cu}_{\text{CP}}$  (black) and bare glassy carbon electrode (GCE, blue) at a scan rate of  $5\text{mV s}^{-1}$  V (vs. RHE). All electrochemical studies were performed in 1M KOH at room temperature.

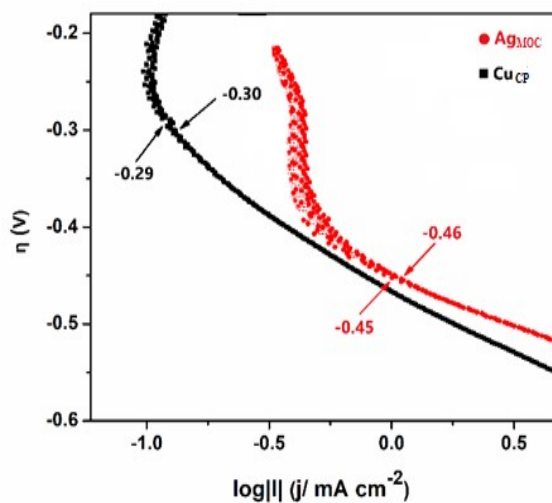


**Fig. S14.** Tafel plot of the  $\text{Ag}_{\text{MOC}}$  and  $\text{Cu}_{\text{CP}}$  indicating onset potential in 1M KOH at room temperature.

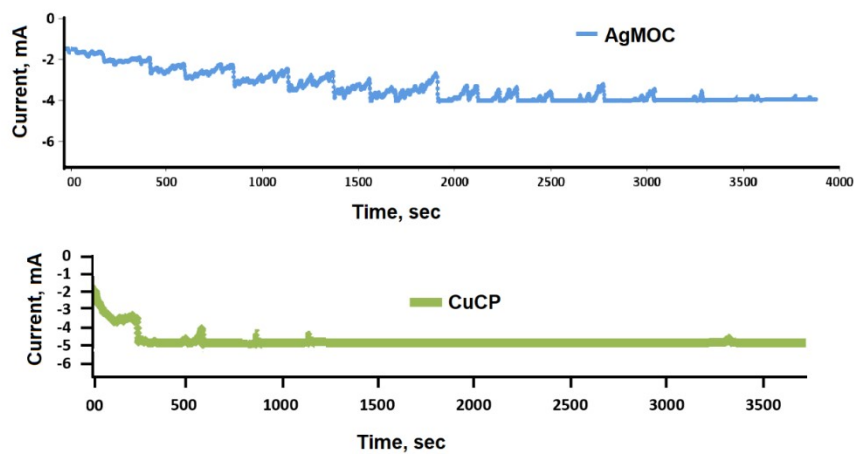


**Fig. S15.** CPE measurement of  $\text{Ag}_{\text{MOC}}$  and  $\text{Cu}_{\text{CP}}$  at a constant potential (-1.65 V vs Ag/AgCl) in 1M KOH media.

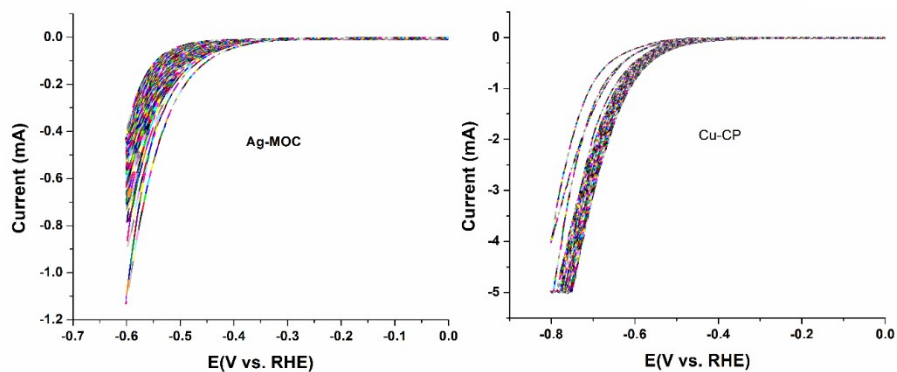


**Fig. S16.** Multiple CVs cycles of  $\text{Ag}_{\text{MOC}}$  and  $\text{Cu}_{\text{CP}}$  in 1M KOH media.

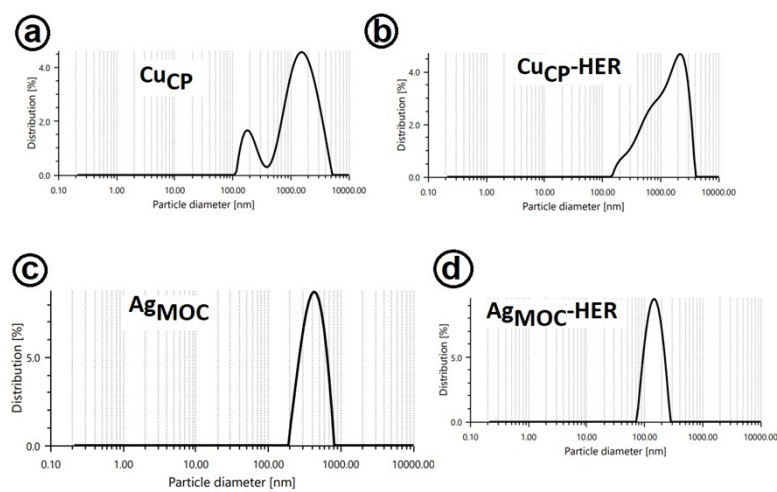


**Fig. S17.** DLS plot of  $\text{Ag}_{\text{MOC}}$  and  $\text{Cu}_{\text{CP}}$  before and after HER study.

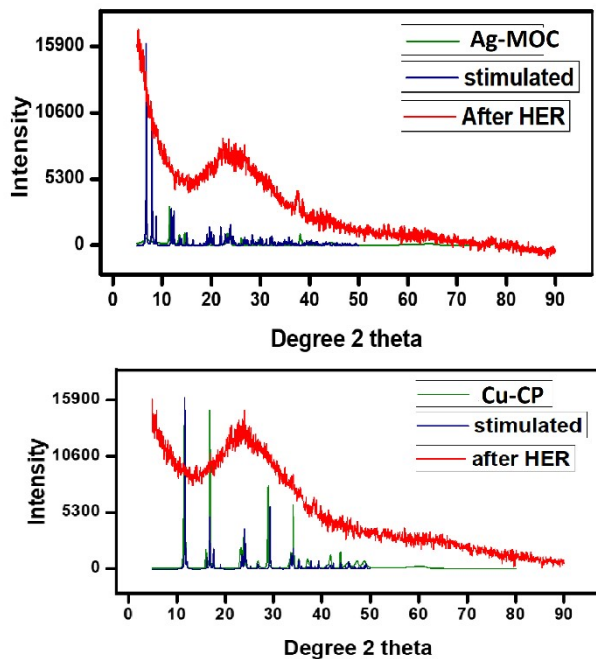


Fig. S18. PXRD diagram of  $\text{Ag}_{\text{MOC}}$  and  $\text{Cu}_{\text{CP}}$  before and after HER study.

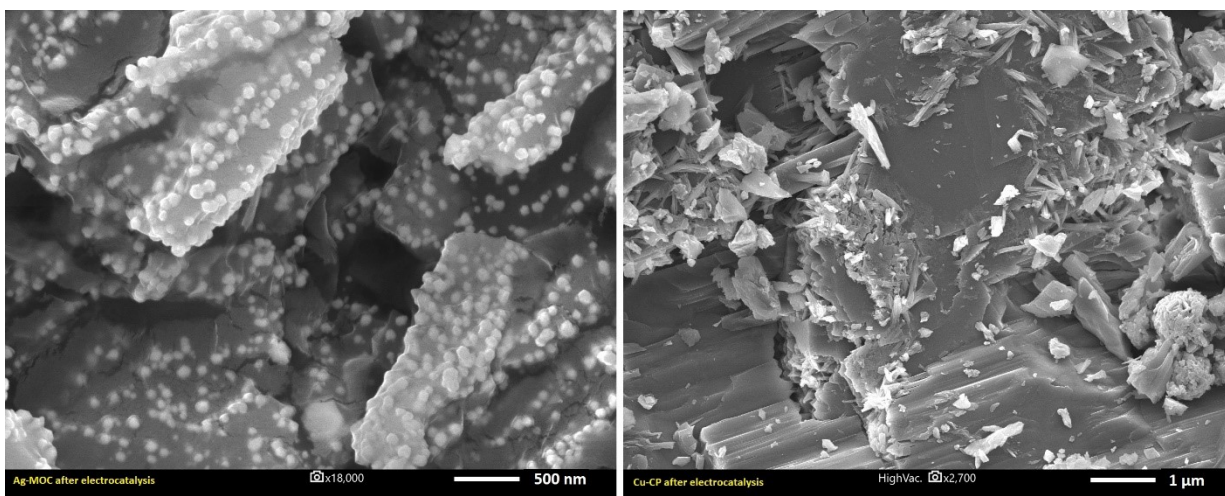
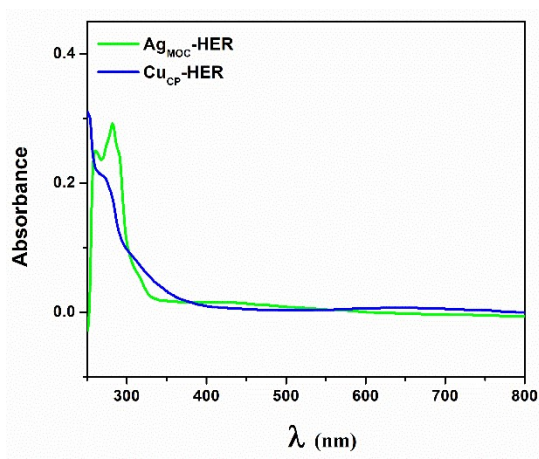
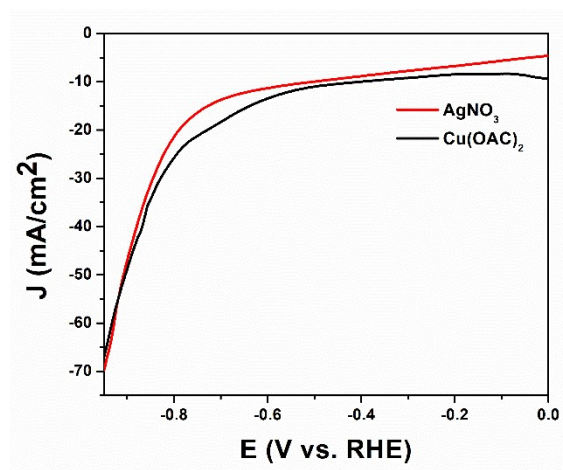


Fig. S19. FESEM images of  $\text{Ag}_{\text{MOC}}$  (left) and  $\text{Cu}_{\text{CP}}$  (right) after HER study.



**Fig. S20.** UV-Vis spectra of the recovered  $\text{Ag}_{\text{MOC}}$  and  $\text{Cu}_{\text{CP}}$  after HER study in DMSO.



**Fig. S21.** LSV of parent metal salts,  $\text{AgNO}_3$  and  $\text{Cu}(\text{OAc})_2$  at 5 mV/s in 1M KOH.

## D. Tables

**Table S1.** Crystallographic structural parameters of  $\text{Ag}_{\text{MOC}}$  and  $\text{Cu}_{\text{CP}}$

Parameters	Ag <sub>MOC</sub>	Cu <sub>CP</sub>
Empirical formula	C <sub>19</sub> H <sub>22</sub> AgN <sub>2</sub> O <sub>3</sub> (NO <sub>3</sub> )	C <sub>3.5</sub> H <sub>5.5</sub> CuN <sub>2</sub> O <sub>1.5</sub> S
Formula weight	496.26	195.20
T (K)	100	293
Wavelength (Å)	0.71073	0.71073
Crystal system	Triclinic	Monoclinic
Space group	P-1(No.2)	I2/a(No.15)
Unit Cell Dimensions		
a (Å)	7.7269(1)	11.4102(5)
b (Å)	12.0436(1)	10.5154(3)
c (Å)	13.6225(2)	12.2122(7)
α (°)	72.750(1)	90
β (°)	87.487(1)	117.067(6)
γ (°)	74.100(1)	90
V (Å <sup>3</sup> )	1163.40(3)	1304.77(12)
Z	1	48
ρ (gcm <sup>-3</sup> )	1.417	1.983
Absorption coefficient (mm <sup>-1</sup> )	0.902	3.583
F(000)	504	774
Theta range for data collection	3.5 to 38.6	3.7 to 31.8°
Index ranges (h, k, l)	-13,13 ; -20,21 ; -23,23	-13,16 ; -14,4 ; -17,14
Reflections collected	12615	4617
Independent reflections	275	136
R(int)	0.068	0.058
Final R indices [I>2sigma(I)]	R <sub>1</sub> = 0.0618, wR <sub>2</sub> = 0.2002	R1 = 0.0381wR2 = 0.1553
Largest diff. peak and hole	-1.20 and 3.49 e. Å <sup>-3</sup>	-0.78 and 0.85 e. Å <sup>-3</sup>

**Table S2.** Bond distance and bond angle values of Ag<sub>MOC</sub> obtained from XRD and DFT

Bond Distances(Å)					
Ag <sub>MOC</sub>	XRD		Ag <sub>MOC</sub>	XRD	

Ag1-N1	2.152(2)		Ag1-N2_a	2.152(2)	
<b>Bond Angles(°)</b>					
<b>Ag<sub>MOC</sub></b>	<b>XRD</b>		<b>Ag<sub>MOC</sub></b>	<b>XRD</b>	
N1-Ag1-N2_a	173.19(9)		Ag1-N1-C8	127.68(19)	
Ag1-N1-C9	115.13(16)		Ag1_a-N2-C11	114.41(16)	
Ag1_a-N2-C12	127.77(18)				

**Table S3.** Bond distance and bond angle values of **Cu<sub>CP</sub>** obtained from XRD and DFT

<b>Bond Distances(Å)</b>					
<b>Cu<sub>CP</sub></b>	<b>XRD</b>		<b>Cu<sub>CP</sub></b>	<b>XRD</b>	
Cu01-O003	1.9061(13)		Cu01-N005	1.961(4)	
Cu01-O004	1.963(2)		Cu01-N007_a	2.009(3)	
Cu01-S002_c	2.7858(11)				
<b>Bond Angles(°)</b>					
<b>Cu<sub>CP</sub></b>	<b>XRD</b>		<b>Cu<sub>CP</sub></b>	<b>XRD</b>	
O003 -Cu01-O004	94.39(11)		Cu01_a -O003 -C00B	113.84(9)	
O003 -Cu01 -N005	172.17(11)		Cu01-O004 -C006	133.5(2)	
O003-Cu01 -N007_a	84.57(15)		Cu01 -N005 -C009	158.3(2)	
S002_c-Cu01 -O003	89.78(3)		Cu01_a -N007 -C00A	108.9(3)	
O004 -Cu01 -N005	89.97(10)		Cu01_a -N007 -H00A	110.00	
O004-Cu01 -N007_a	167.36(14)		Cu01_a -N007 -H00B	110.00	
S002_c -Cu01 -O004	95.89(7)		Cu01 -O003 -C00B	93.62(17)	
N005-Cu01 -N007_a	89.76(14)		Cu01_d -S002 -C009	96.97(13)	
S002_c-Cu01 -N005	96.25(10)		Cu01 -O003 -C00B	113.84(9)	
S002_c -Cu01 -N007_a	96.71(12)		Cu01 -O003 -Cu01_a	132.33(17)	

**Table S4:** Schottky Diode Parameters.

Sample	d(V)/d(lnI) vs. I Graph		H(I) vs. I Graph	
	Ideality Factor ( $\eta$ )	Series Resistance ( $R_s$ ) ( $\Omega$ )	Barrier Height ( $\phi_b$ ) (eV)	Series Resistance ( $R_s$ ) ( $\Omega$ )
<b>Cu<sub>CP</sub></b>	1.31	547.19	0.63	520.50
<b>Ag<sub>MOC</sub></b>	1.17	348.05	0.59	298.26

**Table S5:** SCLC/Charge Transport Parameters

Sample	Dielectric constant ( $\epsilon_r$ )	Carrier mobility ( $\mu$ ), $\text{m}^2\text{v}^{-1}\text{s}^{-1}$	Transit Time ( $\tau$ ) (Sec)
<b>Cu<sub>CP</sub></b>	4.09	$5.90 \times 10^{-6}$	$4.25 \times 10^{-8}$
<b>Ag<sub>MOC</sub></b>	8.85	$1.23 \times 10^{-5}$	$2.04 \times 10^{-8}$

**Table S6.** HER performance parameters

Catalyst	Current density ( $j$ , $\text{mA cm}^{-2}$ )	Overpotential ( $\eta$ , mV)	Tafel Slope ( $\text{mV dec}^{-1}$ )	Electrolyte
<b>Ag<sub>MOC</sub></b>	10	550	104	1M KOH
<b>Cu<sub>CP</sub></b>	10	594	128	1M KOH

## References

- [1] Bruker. SMART (Version 5.0) and SAINT (Version 6.02), Bruker AXS Inc., Madison, WI, USA (2000).
- [2] G.M. Sheldrick, SADABS, Program For Empirical Correction of Area Detector Data, University of Gottingen, Germany, 2000.
- [3] G.M. Sheldrick, SHELXS97 and SHELXL97, Program For Crystal Structure Refinement, University of Gottingen, Germany, 1997
- [4] X. Huang, H. Yao, Y. Cui, W. Hao, J. Zhu, W. Xu, D. Zhu, Conductive Copper Benzenehexathiol Coordination Polymer as a Hydrogen Evolution Catalyst. *ACS Appl. Mater. Interfaces*, 2017, **9** (46), 40752–40759.
- [5] R. Z. Zhang, L. Le Lu, Z. H. Chen, X. Zhang, B. Y. Wu, W. Shi, P. Cheng, Bimetallic Cage-Based Metal–Organic Frameworks for Electrochemical Hydrogen Evolution Reaction with Enhanced Activity. *Chem. - A Eur. J.* 2022, **28** (28), e202200401.
- [6] E. H. Roderick and R. H. Williams, *Clarendon Press, Oxford, 2nd edn*, 1988.
- [7] S. M. Sze, *Wiley*, New York., 1981.
- [8] S. Sil, R. Jana, A. Biswas, D. Das, A. Dey, J. Datta, D. Sanyal and P. P. Ray, *IEEE Trans. Electron Devices*, 2020, **67**, 2082-2087.
- [9] M. Das, J. Datta, A. Dey, R. Jana, A. Layek, S. Middya and P. P. Ray, One step hydrothermal synthesis of a rGO–TiO<sub>2</sub> nanocomposite and its application on a Schottky diode: improvement in device performance and transport properties *RSC Adv.*, 2015, **5**, 101582-101592, <https://doi.org/10.1039/C5RA17795B>.
- [10] S. Middya, A. Layek, A. Dey, J. Datta, M. Das, C. Banerjee and P.P. Ray, Role of zinc oxide nanomorphology on Schottky diode properties, *Chem. Phys. Lett.*, 610 (2014) 39-44, <https://doi.org/10.1016/j.cplett.2014.07.003>
- [11] D Das, M Das, S Sil, P Sahu, and P.P. Ray, Effect of Higher Carrier Mobility of the Reduced Graphene Oxide–Zinc Telluride Nanocomposite on Efficient Charge Transfer Facility and the Photodecomposition of Rhodamine B, *ACS Omega* 2022, **7**, 26483–26494, <https://doi.org/10.1021/acsomega.2c02472>.

[12] J. Datta, M. Das, S. Sil, S. Kumar, A. Dey, R. Jana, S. Bandyopadhyay and P. P. Ray, *Mater. Sci. Semicond. Process.*, 2019, **91**, 133–114.